

Figure S1. *etv2* and *prox1a* are co-expressed in lymphatic progenitors in the posterior cardinal vein, parachordal lymphangioblasts, and the thoracic duct.

Confocal imaging analysis of live embryos and larvae. TgBAC(*etv2*:GFP) and *prox1a*:RFP are co-expressed in lymphatic progenitors (arrow/dashed lines) in the PCV at 24 hpf (A-D, projection of 3 axial positions) and the thoracic duct and intersegmental lymphatic vessels at 4.5 dpf (E-H). (B-D and F-H) show magnified regions indicated by boxes in (A,E). Embryos and larvae have been analyzed from 2 independent experiments. DA, dorsal aorta; PCV, posterior cardinal vein; TD, thoracic duct; ISLV, intersegmental lymphatic vessel.

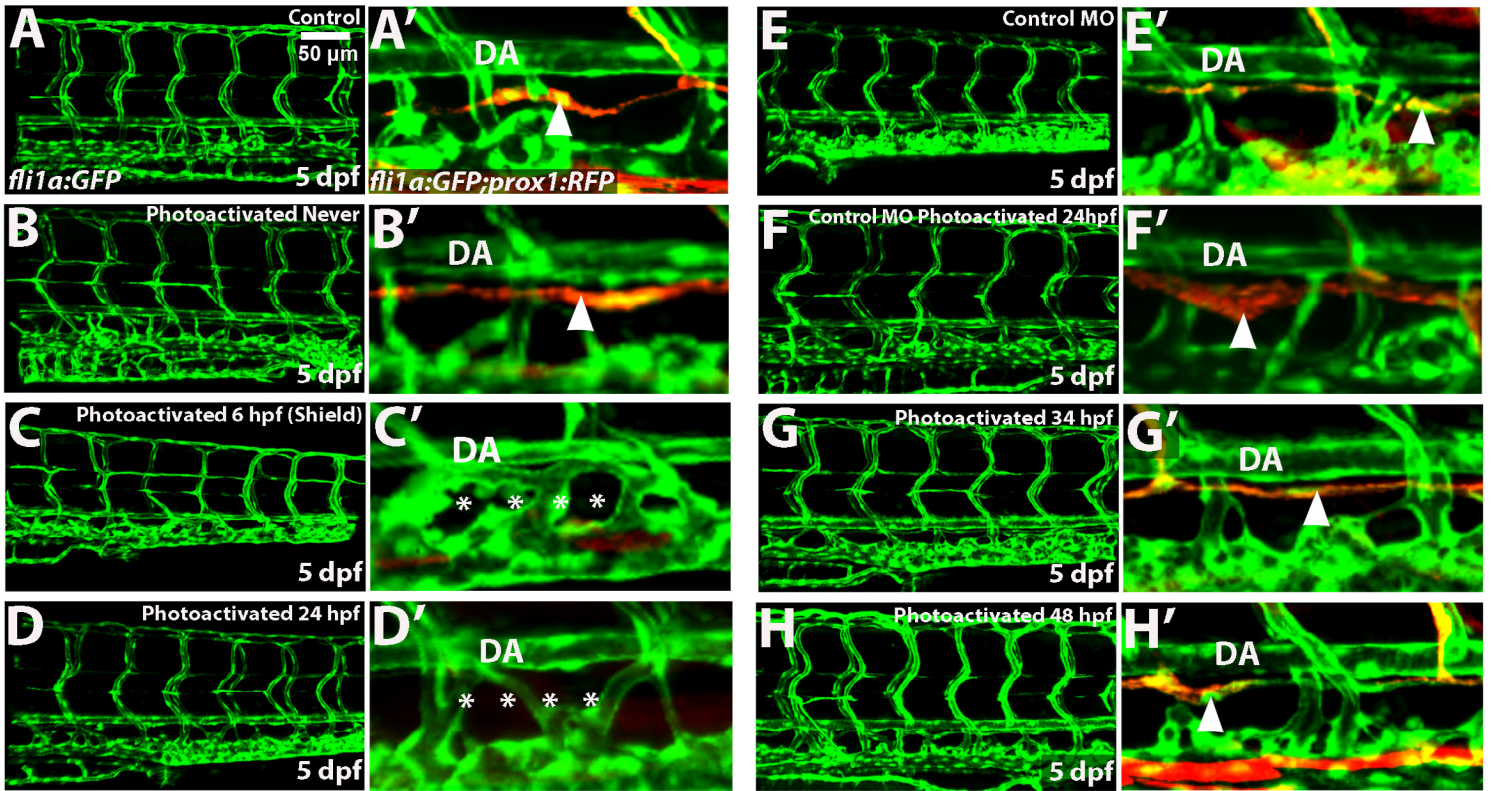


Figure S2. Caged *etv2* MO photoactivation at 24 hpf but not at the later stages specifically inhibits thoracic duct formation as analyzed by confocal imaging of *fli1a:GFP*; TgBAC(*prox1a:KaIt4-UAS:uncTagRFP*) larvae at 5 dpf.

(A-H) Images of the trunk region in the GFP channel (left panels) and enlarged views of the thoracic duct in GFP and RFP channels (A'-H'). DA, dorsal aorta.

(A-D) Caged *etv2* MO photoactivation at 24 hpf results in the absence of the thoracic duct. Note the normal vascular patterning and present thoracic duct (arrowhead) in uninjected control and never photoactivated larvae (A,A',B,B'), abnormal vascular patterning and absent thoracic duct in the early uncaged larvae (shield stage, 6 hpf) (C, C', asterisks) and normal vascular patterning and absent thoracic duct when *Etv2* function was inhibited at 24 hpf (D, D', asterisks).

(E,F) Injection and photoactivation of the standard control MO and *etv2* caging strand mixture does not affect vascular patterning or thoracic duct formation (arrowhead). (E,E') Standard control MO / *etv2* caging strand mixture injected larvae which were not photoactivated; (F,F') larvae that were photoactivated at 24 hpf.

(G,H) Photoactivation of caged *etv2* MO injected embryos at 34 hpf (G,G') or 48 hpf (H,H') does not affect thoracic duct formation (arrowheads). Experiment has been replicated at least twice.

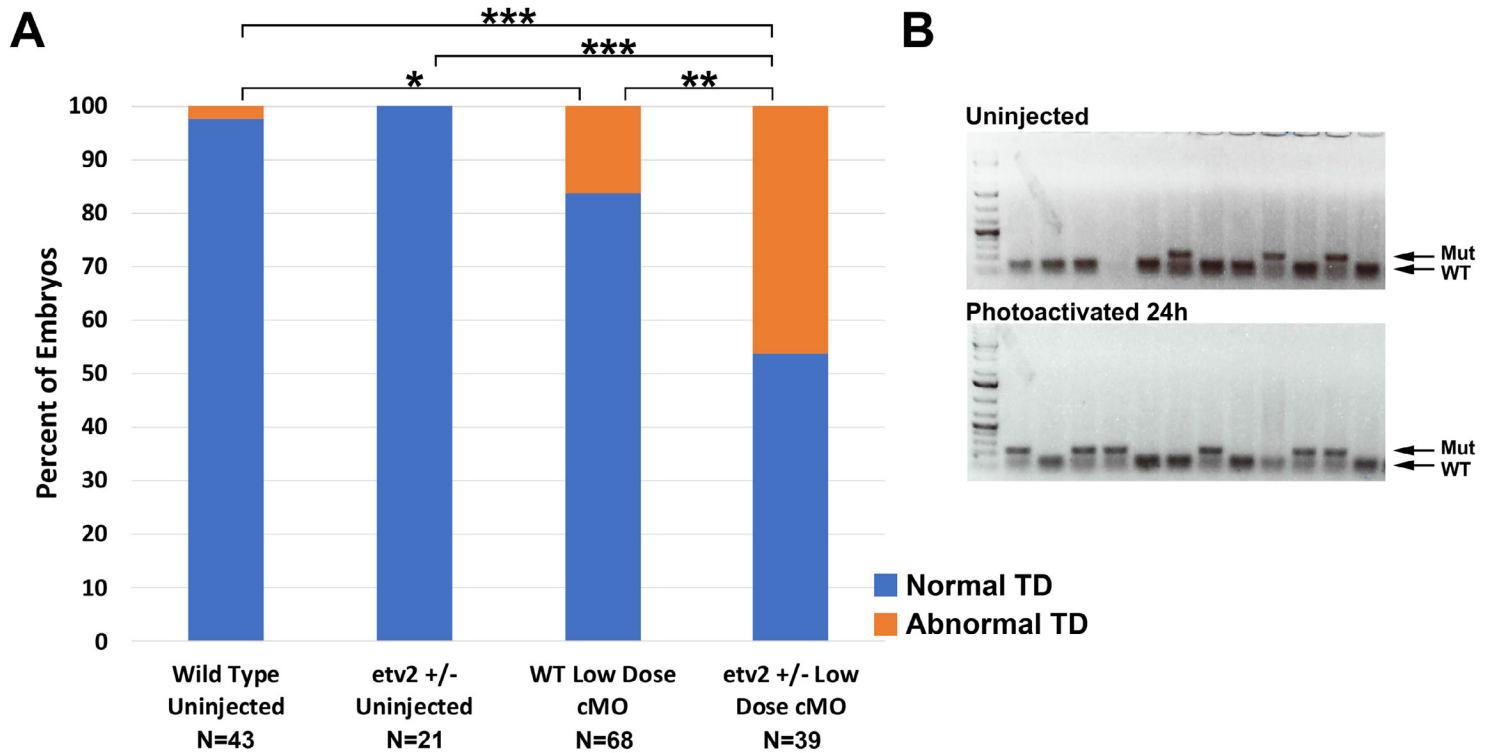


Figure S3. Analysis of the thoracic duct formation in wild-type and *etv2*^{y11} heterozygous larvae injected with reduced doses of caged *etv2* MO.

Progeny from a cross between wild type *fli1a:GFP* and *etv2*^{+/-}; *fli1a:GFP* parents were injected with a reduced dose of caging strand / *etv2* MO mixture. MO was photoactivated at 24 hpf, and larvae were analyzed at 5.5 dpf for the thoracic duct (TD) presence based on *fli1a:GFP* expression and then genotyped. (A) 46% of *etv2*^{+/-} larvae injected with caged MO demonstrated abnormal thoracic duct development compared to 16% of wild type larvae injected with caged MO, 2% of wild type uninjected larvae, and 0% of *etv2*^{+/-} uninjected embryos. (B) A sample gel from genotyping PCR product with BspTI restriction enzyme. PCR product from wild type allele is fully digested while *etv2*^{+/-} allele shows the presence of undigested band and digested products. *, p<0.05 ** p<0.01 *** p<0.001, two-tailed Fisher's exact test. Experiment has been replicated 3 times.

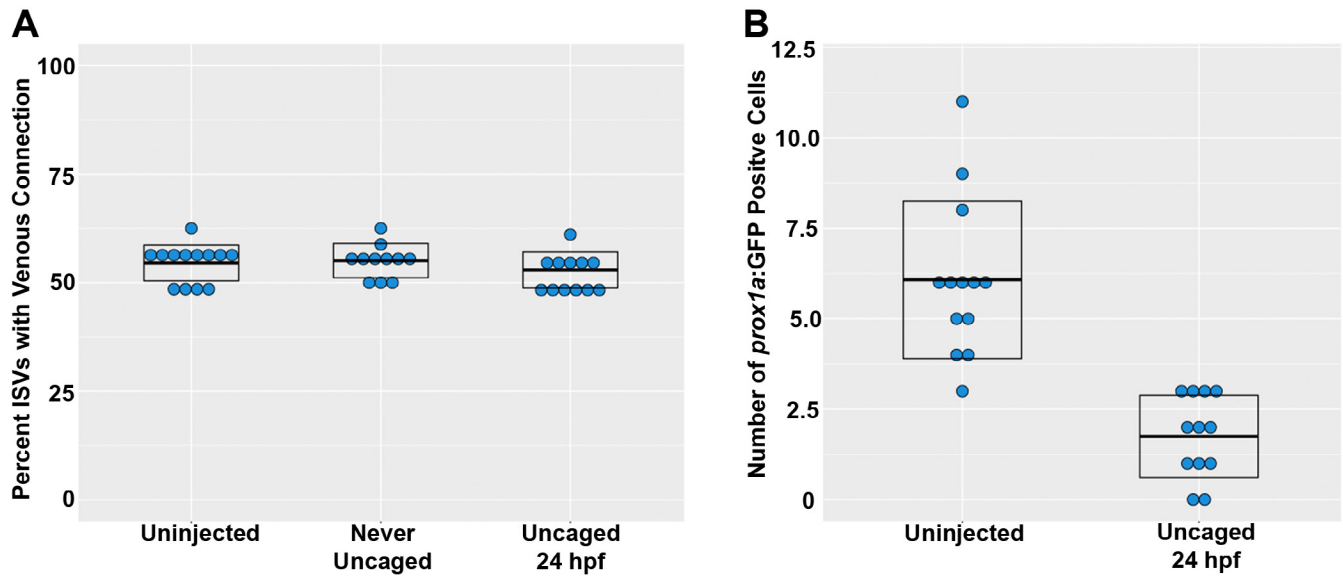


Figure S4. Supplemental data plots that show individual data points for Figures 4D (panel A) and 5C (panel B). (A) Quantification of percent of ISVs with venous connection at 4 dpf. (B) Quantification of *prox1a:GFP* cells at 32 hpf. Each dot represents a single embryo. Boxes represent mean value and standard deviations.

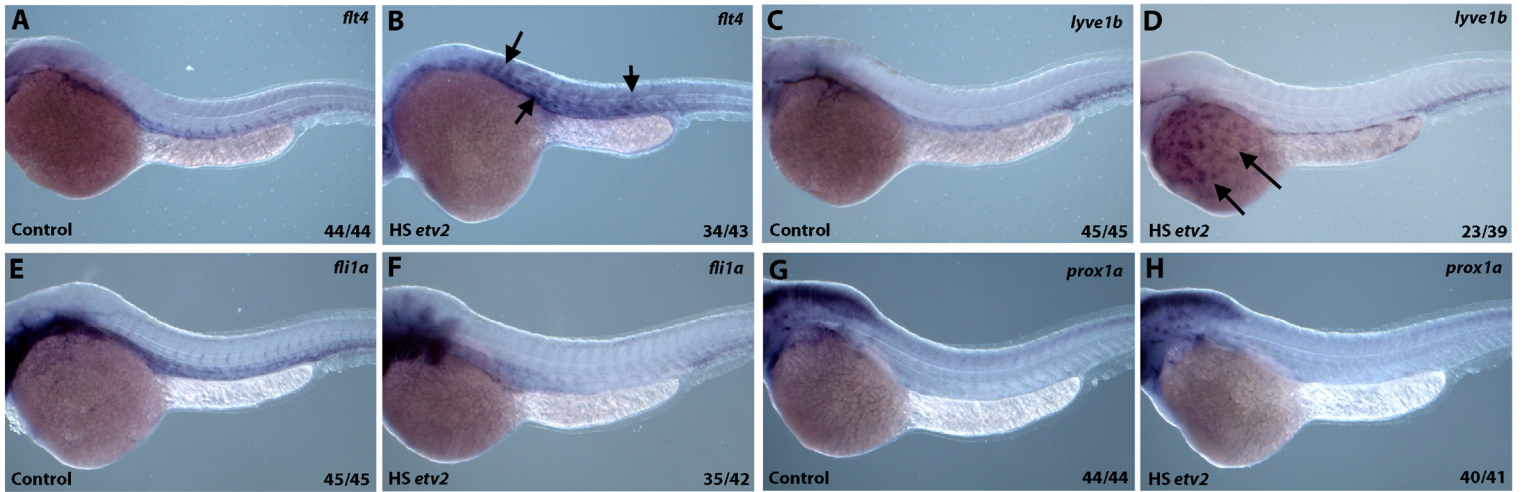


Figure S5. Heatshock inducible overexpression of Etv2 induces ectopic *flt4* and *lyve1b* expression.

(A,B) Embryos injected with *hsp70:etv2-mCherry* overexpression construct show ectopic induction of *flt4* (B) in the somites (arrows) following the heat-shock compared to uninjected controls (A). (C,D) Ectopic expression of *lyve1b* over the yolk is apparent in a subset of embryos that overexpress *hsp70:etv2-mCherry* (arrows, D). (E-H) No ectopic induction of *fli1a* (E,F) or *prox1a* (G,H) was apparent in the embryos that overexpress *hsp70:etv2-mCherry*. All embryos are at 52-54 hpf.

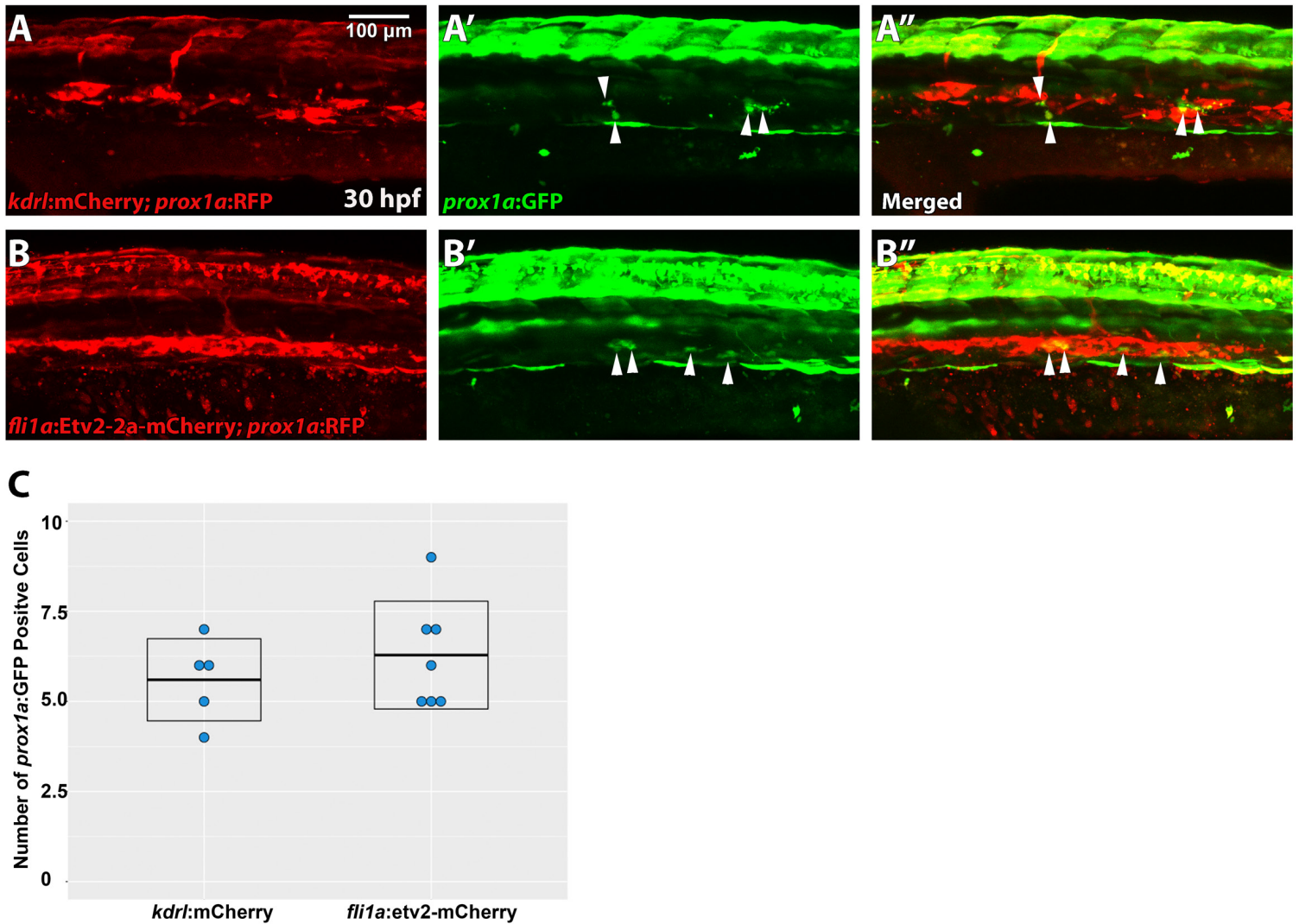


Figure S6. Vascular specific overexpression of Etv2 does not result in expansion of lymphatic progenitors.

Injection of *fli1a:etv2-2a-mCherry* (B-B'') does not result in expansion of *prox1a:GFP*⁺ cells (arrowheads) *etv2* at 30hpf (5.6 ± 0.5 , n=5) compared to control injection of *kdr:mCherry* (A-A') (6.3 ± 0.6 , n=7). Quantification of number of *prox1a*⁺ cells in the vasculature (C) (two-tailed Student's t test $p = 0.41$). Mean \pm SEM is shown. Experiment has been repeated twice.

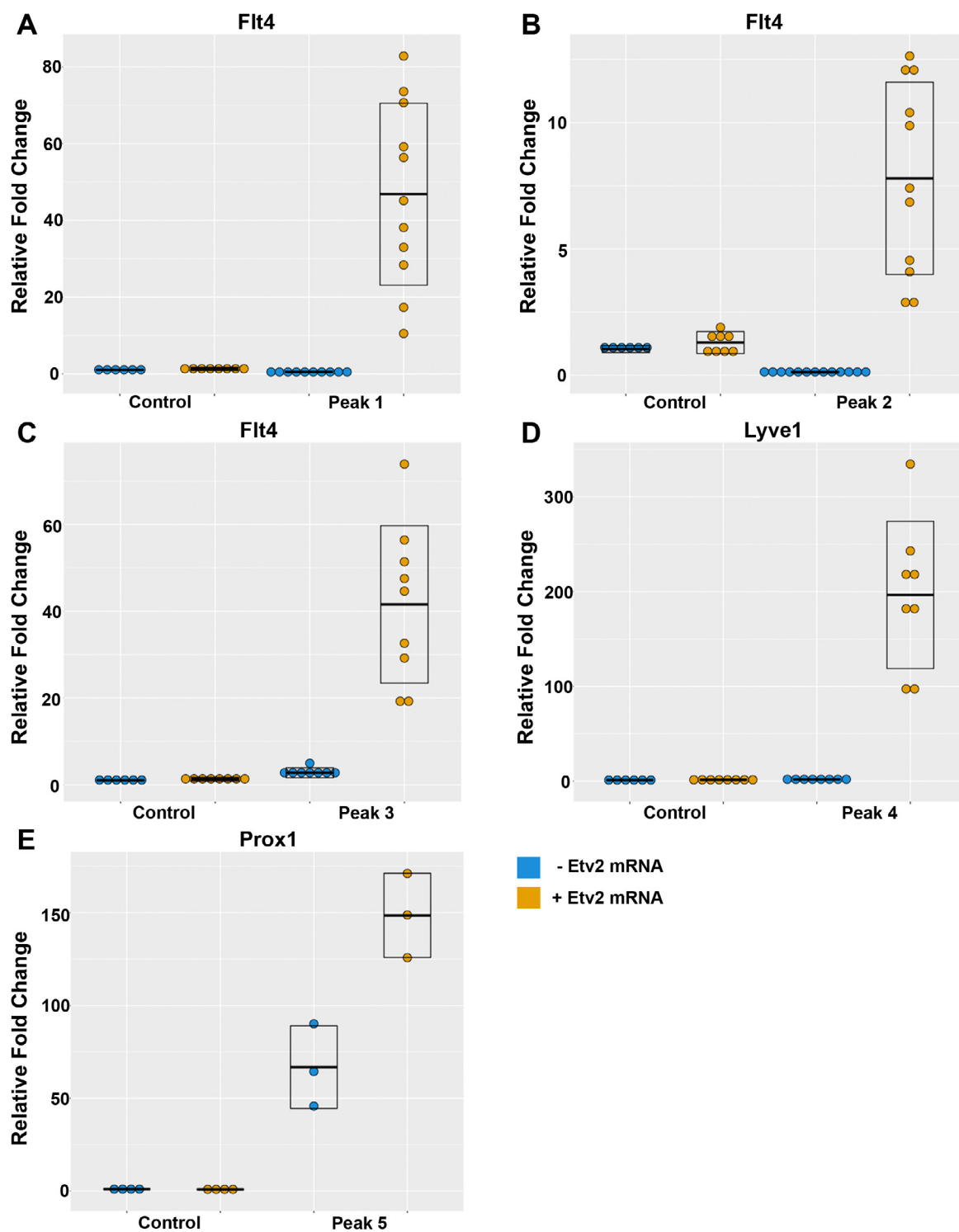


Figure S7. Supplemental data plots for Figure 9B showing individual data points. The graph shows relative luciferase activity in 293T cells of each reporter construct containing the Etv2 peak region (1-5) over pGL4.24 control reporter in the presence or absence of Etv2 expression plasmids (pMSCV-Etv2). Boxes represent mean and standard deviation.

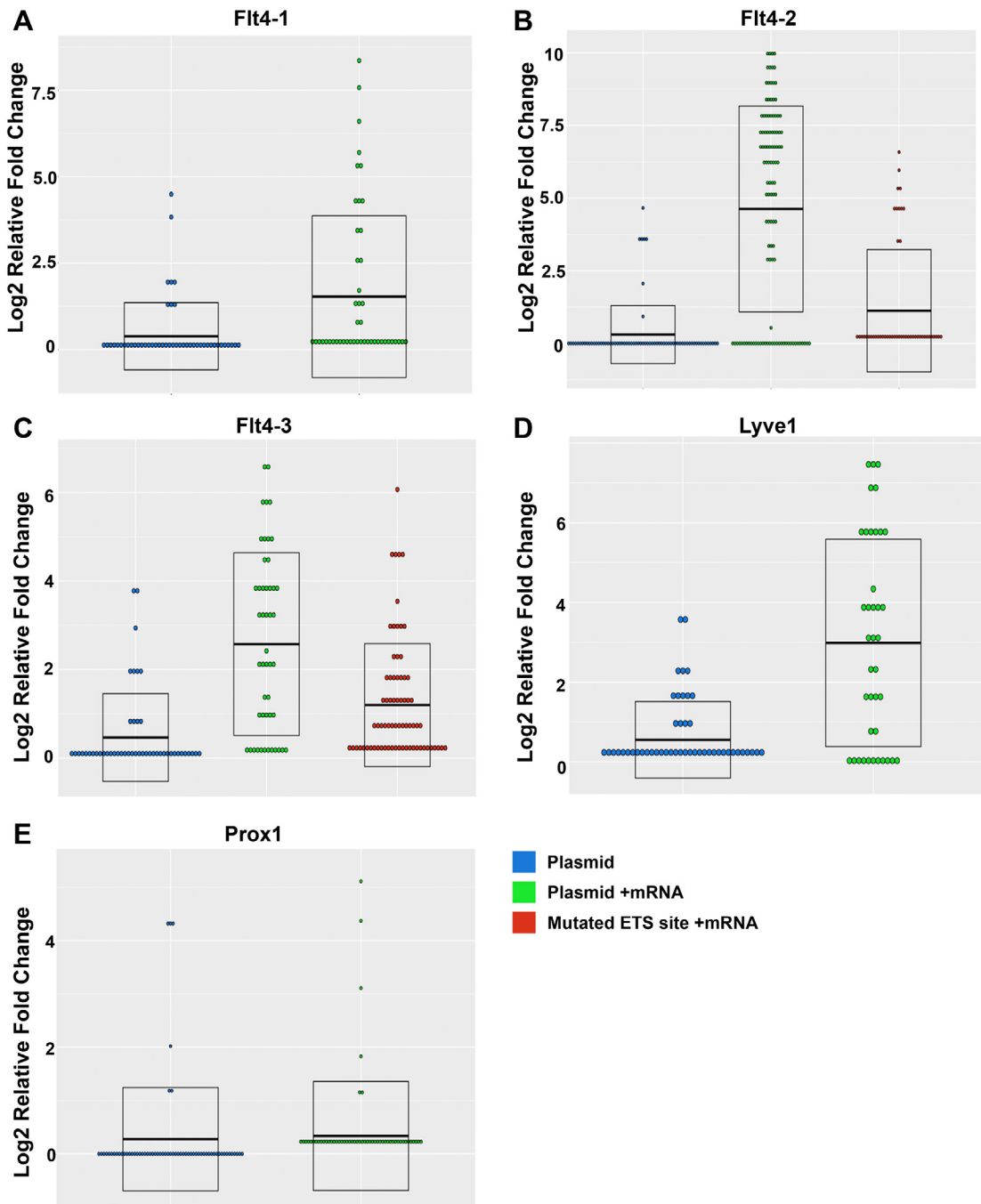


Figure S8. Supplemental data plots for Figure 9C showing individual data points. Graphs show relative luciferase activity for each reporter construct as used in (B) injected in zebrafish larvae with and without zebrafish *etv2* mRNA compared to constructs with mutated ETS binding sites injected together with *etv2* mRNA. Each data point corresponds to a single zebrafish embryo. Note that there is normally a significant variation between embryos and that *etv2* induces ectopic marker expression only in a fraction of embryos. The scale on y axis is based on the log2 values of luminescence intensity. Boxes represent mean and standard deviation.

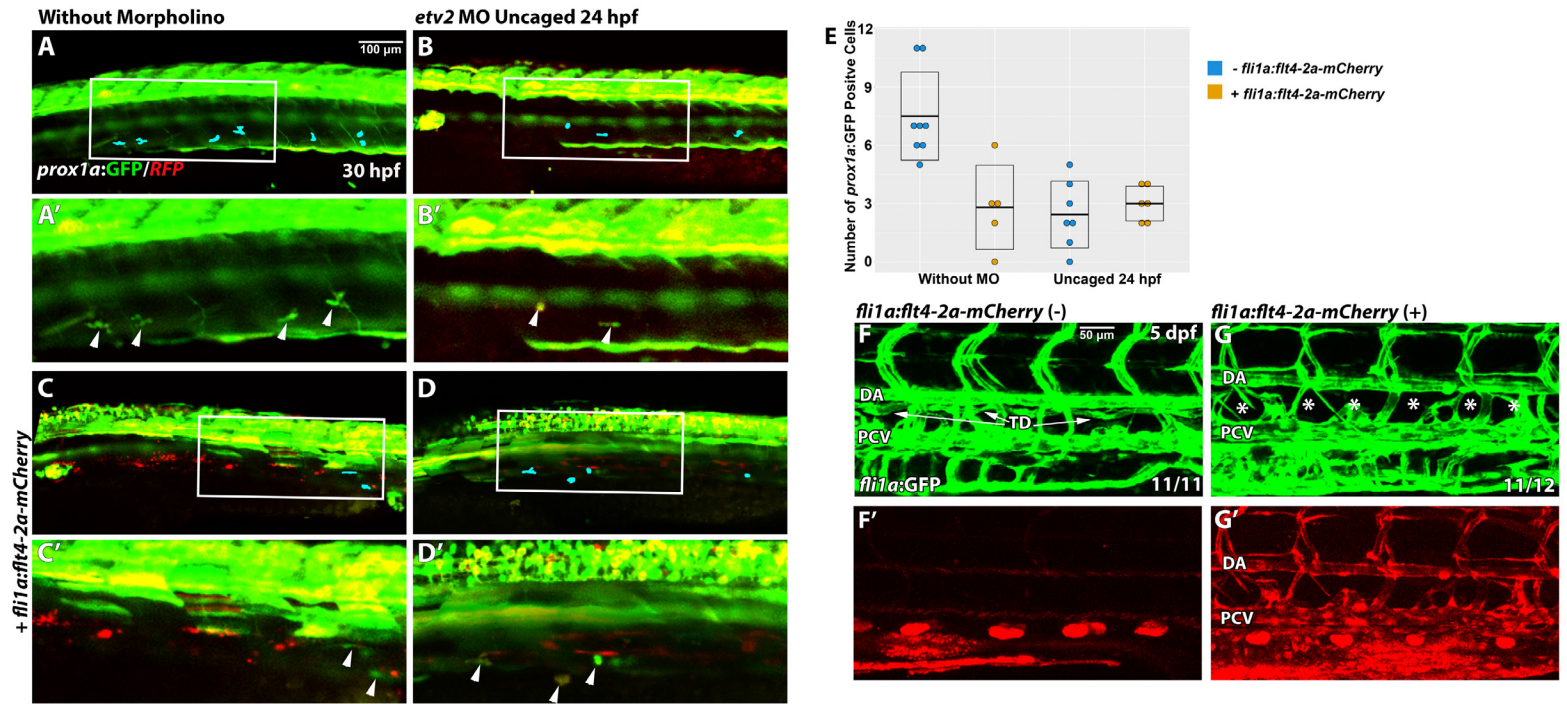


Figure S9. Vascular specific overexpression of Flt4 is not sufficient to rescue lymphangiogenesis defects in photoactivated *etv2* knockdown embryos.

(A,B) The number of lymphatic *prox1a:GFP* cells is reduced at 30 hpf in embryos injected with *etv2* Photomorph solution and photoactivated at 24 hpf (2.4 ± 0.6 , $n=7$) compared to control uninjected embryos (7.5 ± 0.8 , $n=8$, $p < 0.001$, two-tailed Student's test). Note that *prox1a* reporter expresses both RFP and GFP.

(C) Injection of *fli1a:flt4-2a-mCherry* results in a reduction of the number of *prox1a:GFP*⁺ cells at 30 hpf in wild type embryos (2.8 ± 1.0 , $n=5$, $p=0.004$).

(D) Co-injection of *fli1a:flt4-2a-mCherry* together with *etv2* Photomorph solution followed by photoactivation at 24 hpf results in a reduced number of *prox1a:GFP* cells (3 ± 0.4 , $n=6$, $p=0.48$ compared with the injection of *etv2* Photomorph alone, panel B). (A',B',C',D') are higher magnification images of (A,B,C,D).

(E) Quantification of *prox1a:GFP* cell number in the trunk region (across 9 somite length) in different groups. Each data point corresponds to the cell number in a single embryo. Mean \pm SEM values are shown. Arrowheads or blue pseudocolor indicate *prox1a:GFP*⁺ cells within the PCV.

(F,G) Stable transgenic *fli1a:flt4-2a-mCherry* larvae (G,G') have defective thoracic duct development at 5 dpf compared to *fli1a:GFP* larvae (F,F'). Each experiment has been repeated a minimum of two times.

MOVIE LEGENDS

Movie 1. Parachordal lymphangioblast migration and venous sprouting in a wild-type embryo.

Time-lapse imaging of *fli1a*:GFP; *kdr*:mCherry embryo from 30 hpf to 60 hpf demonstrates normal migration of parachordal lymphangioblasts as well as venous sprouting. Arrowheads indicate selected venous sprouts that become venous ISVs or parachordal lymphangioblasts.

Movie 2. Parachordal lymphangioblast migration is inhibited in Etv2 depleted embryos while venous sprouting is unaffected.

Time-lapse imaging of *fli1a*:GFP; *kdr*:mCherry embryo depleted of *etv2* at 24 hpf from 30 hpf to 75 hpf demonstrates a near complete loss of parachordal lymphangioblast (PL) migration and development (asterisks) while venous sprouting is unaffected. White arrowheads indicate venous ISV sprouts or PL sprouts which have reached the horizontal myoseptum. Blue arrowheads indicate stalled or collapsing sprouts, which presumably correspond to lymphatic-fated vessels. In the cases where PL sprouts have reached the myoseptum, their migration along the myoseptum appears to be inhibited.